Negative Effects of Inorganic Salt Invasion on the Dissociation Kinetics of Silica-Confined Gas Hydrate via Thermal Stimulation

Fang, Bin; Lü, Tao; Cheng, Liwei; Wang, Dongdong; Ni, Yang; Fan, Bowen; Meng, Jiuling; Vlugt, Thijs J.H.; Ning, Fulong

DOI
10.1021/acs.energyfuels.2c00978

Publication date
2022

Document Version
Final published version

Published in
Energy and Fuels

energy&fuels

pubs.acs.org/EF

Article

Negative Effects of Inorganic Salt Invasion on the Dissociation Kinetics of Silica-Confined Gas Hydrate via Thermal Stimulation

Bin Fang, Tao Lü,* Liwei Cheng, Dongdong Wang, Yang Ni, Bowen Fan, Jiuling Meng, Thijs J. H. Vlugt, and Fulong Ning*

Cite This: *Energy Fuels* 2022, 36, 6216–6228

Read Online

ACCESS | Metrics & More | Article Recommendations | Supporting Information

ABSTRACT: Methane hydrate dissociation kinetics can be inhibited in NaCl solutions; however, this effect is reversed by promoting bubble formation that enhances dissociation. The negative and positive effects of inorganic salt injection on gas production from hydrate-bearing sediments are still controversial. Here, molecular dynamics simulations were performed to investigate the characteristics of NaCl solution invasion into hydrate-occupied nanopores and the effects on the confined hydrate dissociation kinetics. Two initial configurations comprising liquid and silica pore phases were studied with a low or high NaCl concentration, respectively. The results show that, under the simulation conditions, salt invasion decelerated hydrate dissociation within the silica pore as NaCl invasion into the pore is stepwise. Initially, few ions can diffuse into the pore phase, and gas nanobubbles form on the solid surface mainly via confinement and surface effects, independent of NaCl solution invasion. Subsequently, gradual salt diffusion immersed the residual hydrate in the salt solution and hindered hydrate decomposition until the dissociation finished. More ions could diffuse into the pore phase at the high NaCl concentrations with a low diffusion efficiency, leading to surface nanobubble growth toward the residual hydrate and somewhat accelerated hydrate dissociation. This severely hinders the escape of released methane from the pore. This study yields molecular-level insight into the origin of the negative effect of salt invasion on hydrate dissociation, which should be avoided during gas production from hydrate reservoirs with low permeabilities via salt injection combined with thermal stimulation.

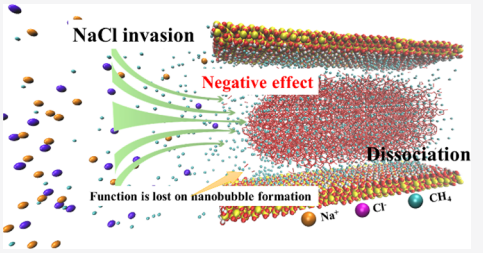

1. INTRODUCTION

Natural gas hydrates (NGHs) are ice-like cage compounds formed by natural gas (mainly methane) and water molecules, wherein the former is captured by cages formed by the hydrogen-bonded network of water.[1] This potential strategic energy resource is estimated to contain double the energy stored in all other fossil fuel deposits;[2] 1 m^3 of saturated gas hydrate decomposes to 164 m^3 of natural gas and 0.8 m^3 of water.[1] NGHs exhibit the characteristics of abundance, clean burning, and low carbon emissions. In nature, most hydrate resources occur in marine sediments and the permafrost regions. In marine sediments, the stability of NGHs is maintained mainly via the pressure of the water layer, and in permafrost regions, the stability of NGHs is realized by the low temperatures. Marine hydrates account for >90% of the global total, most of which are distributed in marine sediments and sedimentary rocks.[3,4] Therefore, marine hydrate reservoirs are key areas in hydrate exploitation. According to the hydrate resource distribution map drawn by Boswell,[5] marine hydrates mostly occur in reservoirs dominated by low-permeability muddy sediments, rendering their exploitation challenging.

The injection of chemical inhibitors is one of the proposed technologies that can be used in gas extraction from marine sediments.[4] This injection may shift the NGH phase equilibrium toward the low-temperature and high-pressure regions, leading to thermodynamically unstable gas hydrates and hindering secondary hydrate formation in the sediments and pipeline after in situ gas-water separation. To increase the gas production efficiency, injection of chemical inhibitors may be combined with other hydrate exploitation methods, such as thermal stimulation[6] and depressurization.[7] NaCl exhibits inhibitory characteristics and is widely used in marine hydrate exploitation because it exhibits little influence on the marine environment and positive effects on gas production from hydrate reservoirs.[8,9] To investigate the mechanism of NaCl solution in hydrate dissociation, Yagasaki et al.[10,11] performed molecular dynamics (MD) simulations to show that the effects of NaCl on hydrate dissociation are complex as deceleration and acceleration effects were observed. In the early stage prior to bubble formation, the NaCl solution decelerates hydrate dissociation because of the increase in the free energy of the aqueous phase with the methane molecules released from the hydrate. This is followed by a faster stage of dissociation via

Received: April 1, 2022
Revised: May 18, 2022
Published: May 27, 2022

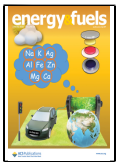

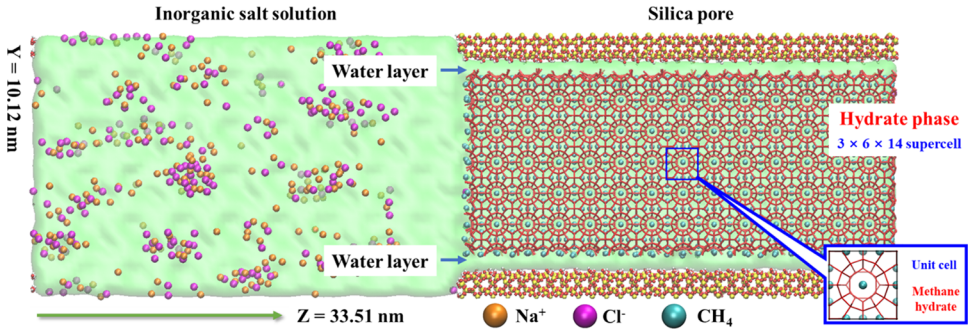

Figure 1. Initial configuration of the simulation cell (using the low concentration system as an example). This simulated system contains four phases: bulk (NaCl solution), pore, and hydrate phases and the water layers. The Si, O, H, and C atoms are shown in yellow, red, white, and cyan, respectively. The hydroxylated (0110) basal planes of silica face the hydrate phase across the water layers.

the facilitation of gas bubble formation. The effects of NaCl, KCl, and $CaCl_2$ electrolyte salt solutions on hydrate dissociation were also analyzed and studied via MD simulations. It was found that all salts facilitate hydrate dissociation by changing the structures of water molecules in the liquid phase. Compared to KCl, $CaCl_2$ and NaCl are more suitable for use in hydrate dissociation based on the energy consumption.[12] Both the positive and negative effects of NaCl addition on hydrate dissociation were observed by experiments, indicating that more complicated physical effects of salts in hydrate dissociation behavior in porous media should be considered, e.g., the dissociation rate and nanobubble formation are considerably influenced by the confined space and physical and chemical properties of the solid surface.[13−15] For example, Nair et al.[6] showed that gas recoveries by thermal stimulation and dissociation rates are lower in porous media formed by silica sands in seawater than those in pure water. Negative effects of salt addition were also reported by Zhuo et al.[16]

To accelerate the industrialization of gas production from hydrate reservoirs, it is important to understand the dynamic response of hydrate dissociation in porous sediments in terms of external conditions. In particular, the effects of salt injection (mainly NaCl, which is a component of seawater) on hydrate dissociation in marine sediments should be well understood. MD simulations are important to interpret experimental observations. Previously, MD simulations have been successfully used to investigate hydrate phase behavior,[17−20] nucleation and growth,[21−29] chemical inhibition,[30−37] transport properties,[38,39] and dissociation behavior.[13,40−47] In this study, MD simulations were performed to investigate the effects of NaCl invasion on hydrate dissociation within silica nanopores in an adiabatic ensemble (NVE). Multiple phase configurations were constructed, such as a bulk phase containing NaCl (at low or high concentrations) and a silica pore phase containing hydrate clusters. Ion invasion into the pores and the effects of ions on the dissociations of hydrate clusters at different concentrations were investigated. This study unravels the molecular origin of the negative effects of NaCl invasion into the pores of methane hydrate in a confined space at a high saturation. This leads to insight into the dissociation behavior of hydrates in sediments so that the negative effects of salts during gas hydrate exploitation can be avoided.

2. MATERIALS AND METHODS

2.1. Simulation Details. The initial configuration consists of a NaCl solution and a nanopore phase, where the NaCl solution is located at the left moiety of the structure as ions (Na^+ and Cl^-) and water. The rest of the configuration is a nanopore phase formed by two hydroxylated silica slabs acting as pore walls. The confined space formed is almost completely occupied by the methane hydrate phase in a cubic shape due to the crystallographic shape of the structure, I. Additionally, between the hydrate cluster and silica slabs, thin water layers (approximately 5 Å) are present because the hydrophilic surface water is constrained and difficult to convert into the hydrate phase,[48] and the addition of a water layer may moderate the mismatch between the silica and hydrate phase.[49−51] The initial configuration shown in Figure 1 approximates the hydrate sediments saturated with the hydrate phase, and no free gas phase exists. For these reasons, a four-phase initial model consisting of a silica pore/hydrate/water/salt solution was constructed.

The unit cell of methane hydrate occurs in structure I and was constructed based on Takeuchi et al.'s work with the Bernal−Fowler rules, with the minimization of the potential energy and dipole moment and a lattice parameter of 12.03 Å.[52] The hydrate cluster consists of 3 × 6 × 14 cubic unit cells in the *xyz* directions. The silica unit cell was extracted from a hexagonal quartz supercell (from the American Mineralogist Crystal Structure Database)[53] into an orthorhombic lattice that was appropriate for use in MD simulations. Each silica slab consists of 7 × 1 × 31 orthorhombic cells with the edge silicon atoms saturated with hydroxyl groups, and the two slabs form the pore phase with a pore size of ∼8.2 nm. Details on constructing the simulation cell are available in previous studies.[13,53] Except for the hydroxyl groups, the atoms in the two silica walls were constrained in the MD simulations, forming immobile substrates on both sides of the hydrate phase. MD simulations were performed at two NaCl concentrations: a low concentration (m) = 0.6 mol/kg, which is the average NaCl concentration of seawater (3.5 wt %), and high concentration (m) = 4.9 mol/kg, which is similar to the experimental saturation conditions at ambient temperature (6 mol/kg). Our previous study performed with pure water was used for comparison.[13] All MD simulations were conducted using the GROMACS package (version 2018, University of Groningen, Groningen, Netherlands), with double precision arithmetic to improve the accuracy of the simulations.[54,55]

Ca. 100,000 atoms were placed in the simulation box with initial dimensions of 3.61 × 10.12 × 33.51 nm (112,525 and 107,197 atoms in the 0.6 and 4.9 mol/kg systems, respectively. The numbers of atoms and molecules for each species are listed in Table 1). The three-site simple point charge/extended SPC/E model was used to describe water molecules. The O−H bond length and H−O−H angle were fixed.[56] Methane molecules were described using the unit atom "optimized potentials for liquid simulations (OPLS)-united atom" force field,[57] and the OPLS force field was also used to describe the Na^+ and Cl^- ions.[58] Silica atoms were described by the interaction potential developed by Lopes et al.[59] Newton's equations of motion

https://doi.org/10.1021/acs.energyfuels.2c00978
Energy Fuels 2022, 36, 6216−6228

Table 1. Number of Molecules or Ions of each Chemical Species in the Two Initial Configurations[a]

	hydrate phase		NaCl solution		
m (mol/kg)	CH_4	H_2O	Na^+	Cl^-	H_2O
0.6	2016	11,592	218	218	22,264
4.9	2016	11,592	1550	1550	19,600

[a] m = NaCl concentration.

were integrated using the leapfrog algorithm with a 1 fs time step.[60] The Lennard-Jones (LJ) potential was used to describe the van der Waals interactions between two atoms with the standard Lorentz−Berthelot mixing rules for dissimilar atoms. The Lennard-Jones and Coulomb interactions (short-range nonbonded interactions) were cut off at 12 Å, with long-range electrostatic interactions described using the particle-mesh Ewald technique.[61] Prior to the MD simulations, to avoid atomic overlaps, the energy of the initial configuration was minimized. Energy minimization was performed using the conjugate gradient algorithm,[62] and short NVT and NPT simulations (200 ps) were performed to relax the temperature and pressure of the system. During the NPT simulation, the equilibrium temperature and pressure were set at 292 K and 3 MPa, respectively. The V-rescale temperature coupling was used to control the system temperature, with a thermostat constant of 0.1 ps. The Parrinello−Rahman extended-ensemble pressure coupling was used to control the pressure, with a barostat constant of 1.0 ps.[63,64] Subsequently, NVE simulations were performed for each system for 50 ns. In all simulations, periodic boundary conditions (PBCs) were applied in all three directions during the simulations.

2.2. Data Analysis. The F_3 order parameter proposed by Baez and Clancy was used to distinguish water molecules in the liquid or solid phase (hydrate and ice).[65] In the solid phase, water molecules are arranged regularly, and their oxygen atoms typically form the vertices of tetrahedral elements with four neighboring water oxygen atoms, which is quite different from the liquid phase. Therefore, based on the O···O···O angle (104.25°),[66] we used the F_3 order parameter to characterize the local states of the water molecules during the MD simulations. The order parameter $F_{3,i}$ for atom i is computed as follows:[65]

$$F_{3,i} = \langle [\cos\theta_{jik}|\cos\theta_{jik}| + \cos^2 104.25]^2 \rangle_{j,k} = \begin{cases} \sim 0.1 & \text{liquid water} \\ \sim 0.0 & \text{solid solid (ice, hydrate)} \end{cases} \quad (1)$$

where θ_{jik} is the O···O···O angle of the specified ith water oxygen atom, with the j and k oxygen atoms adjacent within a spherical radius of 3.5 Å (corresponding to the first minimum in the radial distribution function (RDF) of the water oxygen in the liquid water phase). The brackets ⟨ ⟩ denote a statistical average. Under standard conditions, the average F_3 order parameters are 0.1 and 0 for water in the liquid and solid phases, respectively (hydrate and ice), and this order parameter fluctuates due to atomic thermal motion. In our simulations, we define water in the liquid phase when F_3 is >0.05 and in the hydrate phase when F_3 < 0.05 (H-water). We assume that the methane remains in a hydrate phase (H-methane) if the number of H-water molecules (within the first water shell of methane, 5.5 Å) is >15—otherwise, methane is released into the liquid phase.[10,67]

3. RESULTS

3.1. Hydrate Dissociation Behavior under the NaCl Solution Invasion Effect. In this study, an adiabatic ensemble (NVE) was used in the MD simulations, in which energy and particles cannot be exchanged with the environment. Hydrate dissociation is an endothermic reaction. It should be noted that heat is not a state function, so the heat of a system cannot be increased or decreased. Heat can only be transferred, leading to a large temperature decrease until complete dissociation. As shown in Figure 2, the temperature drops nonlinearly with time because the residual hydrate cluster size is not constant during the simulation, and the system temperature reaches a dynamic equilibrium when the phase change is finished. By comparison, the equilibrium time for the three simulations is different, the time for the pure water system is the shortest, the time for the system with 4.9 mol/kg is the second, and the time for the system with 0.6 mol/kg is the longest. The results indicated that the hydrate dissociation dynamic processes are different, and the details of

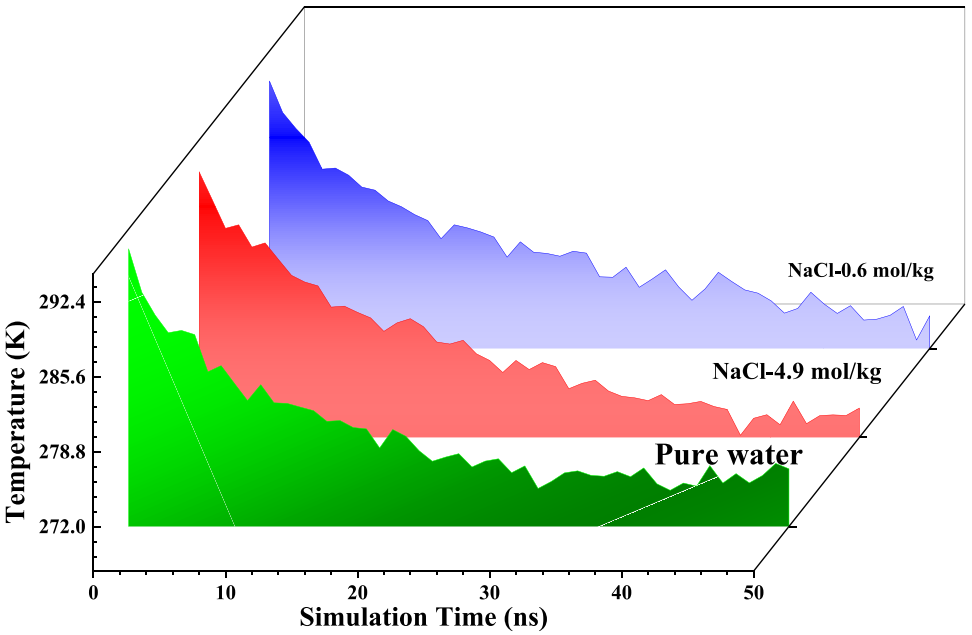

Figure 2. Time evolution of the system temperature profiles of the silica nanopores at different NaCl concentrations. The temperature of the pure water system is obtained from our previous study.[13]

https://doi.org/10.1021/acs.energyfuels.2c00978
Energy Fuels 2022, 36, 6216−6228

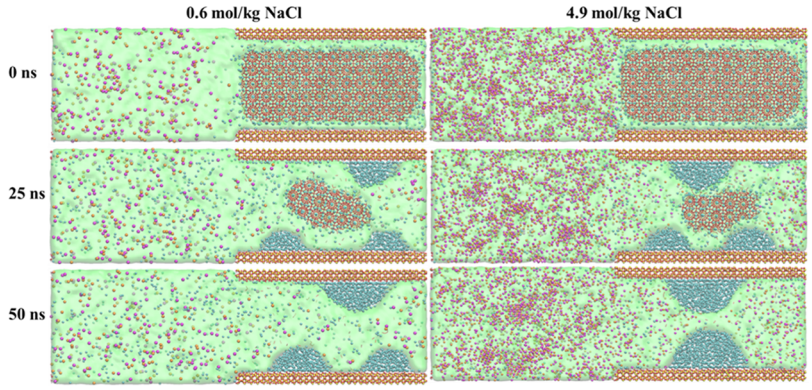

Figure 3. Images of the dissociations of the two systems in the *YZ* planes at different simulation times; atom color settings are the same as Figure 1.

the discussion are shown in Section 3.3. If the reservoir cannot supply the heat lost during the hydrate phase change, then the temperature of the environment may decrease, and a low temperature may decrease the rate of hydrate dissociation. If the temperature decreases below the freezing point, then the formation of an ice-like structure on top of the hydrate surface may limit the heat and mass transfer as a direct consequence of the suspended hydrate dissociation. This is essentially the effect of hydrate self-preservation.[68] In addition, the temperature decrease may again satisfy the temperature−pressure conditions for hydrate formation and induce secondary hydrate formation, which is unfavorable for further hydrate dissociation and blocks gas migration.[69] Therefore, timeous replenishment of heat is critical during gas extraction from hydrate-containing reservoirs.

Based on the calculation of the local order parameter F_3 of water, the water molecules in the solid or liquid phase can be distinguished. As shown in Figure 3, for the dissociation of both systems with different NaCl concentrations, the hydrate clusters form approximate cuboid shapes in the *YZ* plane. The vast majority of guest molecules are located within the H-bonded cages at $t = 0$ ns due to the initial system configuration, with the cages on the surface of the hydrate phase collapsing during the MD simulation equilibration. Similar to the dissociations within silica pores without NaCl or in the liquid phase,[13,65,70,71] the dissociation of hydrate commences at the four acute phases because of the Gibbs−Thomson effect,[72] leading to residual hydrate in an elliptical core. During the hydrate dissociation, the hydrate phase change is layer-by-layer stepwise from outer to central. This is caused by the guest molecules in the interior of the hydrate phase, which are confined within the H-bonded cage, and the hindered diffusion of methane, which may stabilize the H-bonded cage structure. Another contributing factor is the effect of the shielding disturbance of the surrounding water due to the surface-incomplete cage structure, resulting in heterogeneous hydrate dissociation instead of an immediate, complete collapse upon heat stimulation.[73−75] NaCl invasion at different concentrations does not change the hydrate dissociation mechanism.

Hydrate dissociation is a multiphase effect, involving the diffusion of water and methane molecules. The hydrate is high in methane content and is thus a potentially unconventional source of natural gas. As the hydrate dissociates, methane molecules are released from the solid phase to the surrounding liquid, acting as a solute. Due to the large interface between the silica and hydrate across the thin water layers, numerous methane molecules escape from the hydrate surface and diffuse into the thin water layers, driven by the fugacity difference (between the hydrate phase and liquid phase) and diffuse across these water layers. This leads to the aggregation of gas molecules on the solid surfaces due to steric hindrance and the low solubility of methane in water. Gas clusters of methane form on the hydrophilic surfaces of the silica slabs and grow into surface nanobubbles, with no nanobubble formation in the bulk phase. This indicates that the locations of nanobubble formation in the two simulation systems (with a low or high NaCl concentration) are similar to those of the dissociations within silica pores without NaCl.[13]

The hydrate−liquid−gas three-phase equilibrium pressure−temperature curves of hydrates may be shifted toward high pressures and low temperatures by increasing the NaCl concentration,[76] with the pressure−temperature offset depending on the inorganic salt concentration. Generally, inorganic salts act as thermodynamic inhibitors that may hinder hydrate formation and growth and facilitate dissociation.[77] The addition of NaCl outside the pore at low and high concentrations may decelerate the dissociation of the hydrate phase within the silica nanopore compared to that of the non-additive simulation system under the same initial pressure−temperature conditions (Figure 4). The negative effects of

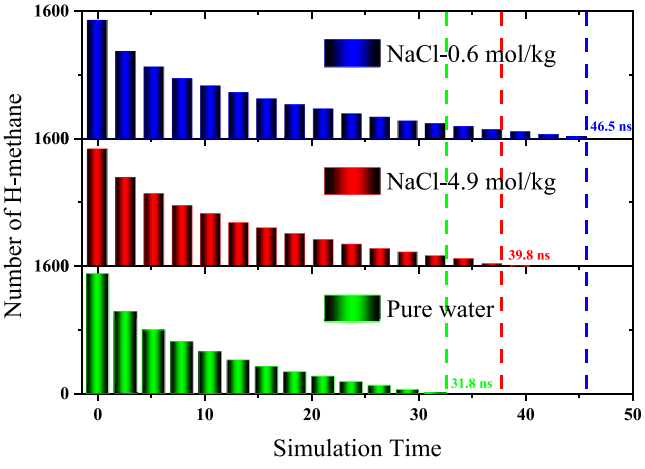

Figure 4. Time evolution of the numbers of methane molecules in the hydrate phases (H-methane) of the three dissociation systems, indicating clearly that the hydrate phase dissociates fastest in the system without NaCl solution.[13] The green, red, and blue dash lines represent the hydrate dissociation completed time for the three systems without and with NaCl solution.

https://doi.org/10.1021/acs.energyfuels.2c00978
Energy Fuels 2022, 36, 6216−6228

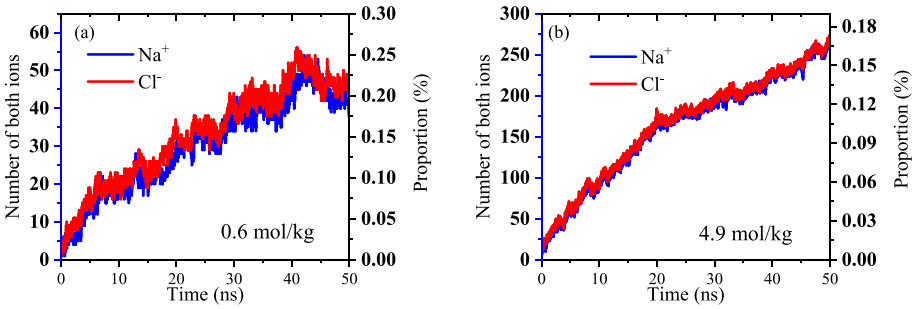

Figure 5. Numbers and proportions of ions diffused into the pores of the two systems in 0.6 mol/kg (a) and 4.9 mol/kg (b) NaCl concentration as a function of the simulation time.

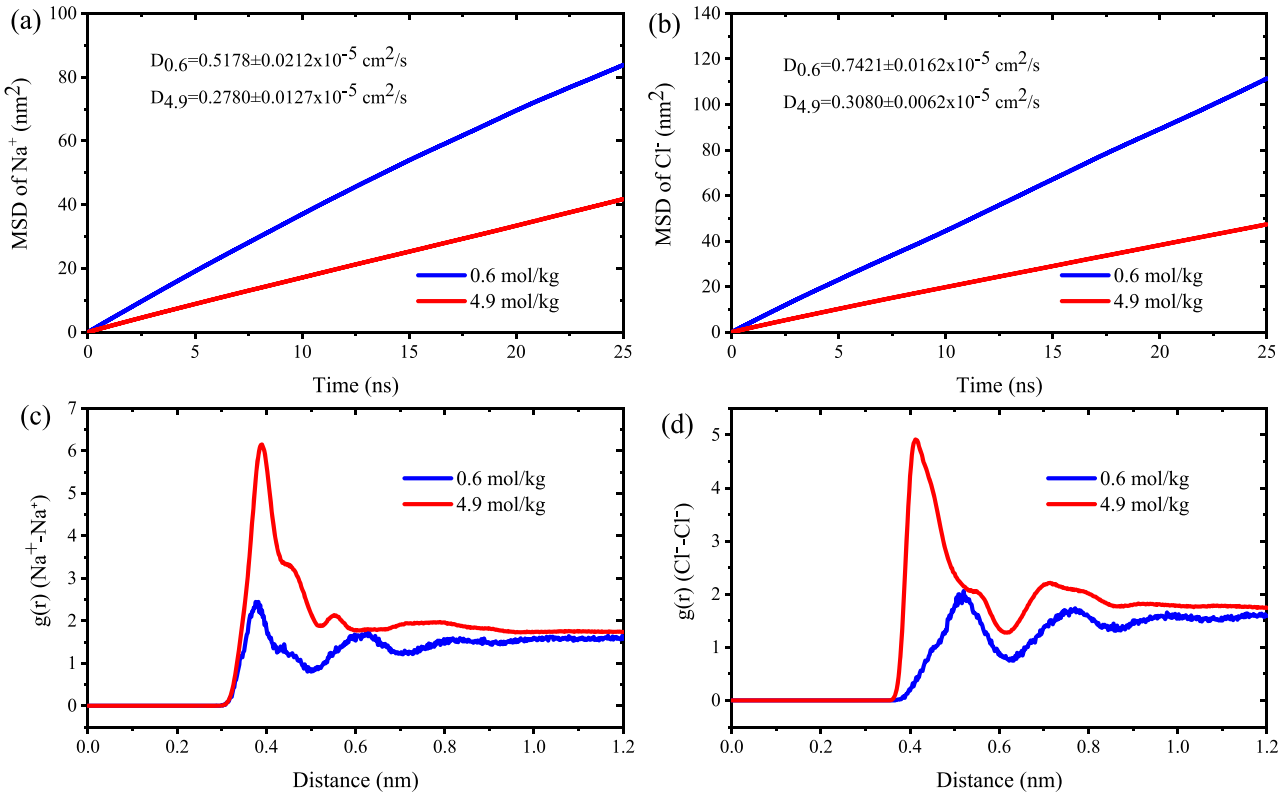

Figure 6. Mean square displacements (MSDs) and radial distribution functions of the Na^+ cation (a, c) and Cl^- anion (b, d) in each simulation system. It should be noted that we ignored the finite-size effects of diffusion coefficients calculation because the two systems are almost the same size.[78]

NaCl on hydrate dissociation are also observed experimentally.[6] To investigate the origin of the negative effects of NaCl on dissociation, the kinetic characteristics of ion invasion from the NaCl solution into the nanopore during hydrate dissociation should be clarified.

3.2. Characteristics of Ion Invasion. At the initial stage of dissociation, the hydrate phase almost completely occupies the pore space with a high saturability, and NaCl is added as an additive to the bulk phase external to the pore and occurs in ionic form (Na^+ and Cl^-). As the hydrate dissociates, the solid phase converts to a liquid, freeing up the pore space, with the ions gradually permeating into the nanopore from the two pore entrances due to the PBC. The numbers of Na^+ and Cl^- ions that diffuse into the pores of the two systems are shown in Figure 5. More ions are observed in the pore phase with a high NaCl concentration in the initial bulk phase, but the ratio of ions diffused into the pore and the total number of ions in the system is less at the same simulation time.

We also calculated the mean square displacements (MSDs) of Na^+ and Cl^- in solution (Figure 6a,b), which indicate that the diffusion may be lowered by increasing the NaCl concentration. In our simulations, although the ion concentration is high (4.9 mol/kg), the ion diffusion coefficient decreases, as calculated using the Einstein relation, and the proportion of ions diffused into the pore is reduced. Therefore, the fraction of the number of ions in the pore decreases with increasing NaCl concentration outside the pore, and thus, small amounts may diffuse into the pore and control the dissociation of the residual hydrate phase. The RDFs of Na^+-Na^+ and Cl^--Cl^- in the two simulation systems are shown in Figure 6, indicating that Na^+ and Cl^- ions generally form ion clusters in the high NaCl concentration solution as opposed to those in the low NaCl concentration solution. This leads to a

https://doi.org/10.1021/acs.energyfuels.2c00978
Energy Fuels 2022, 36, 6216−6228

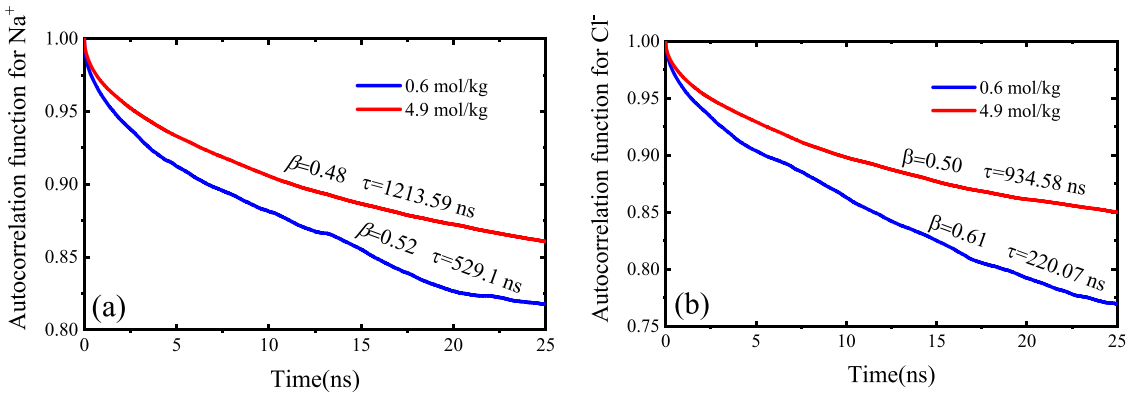

Figure 7. Autocorrelation functions and residence times (τ) of Na^+ (a) and Cl^- (b) of ion diffusion into the pores from the bulk phases in both NaCl systems.

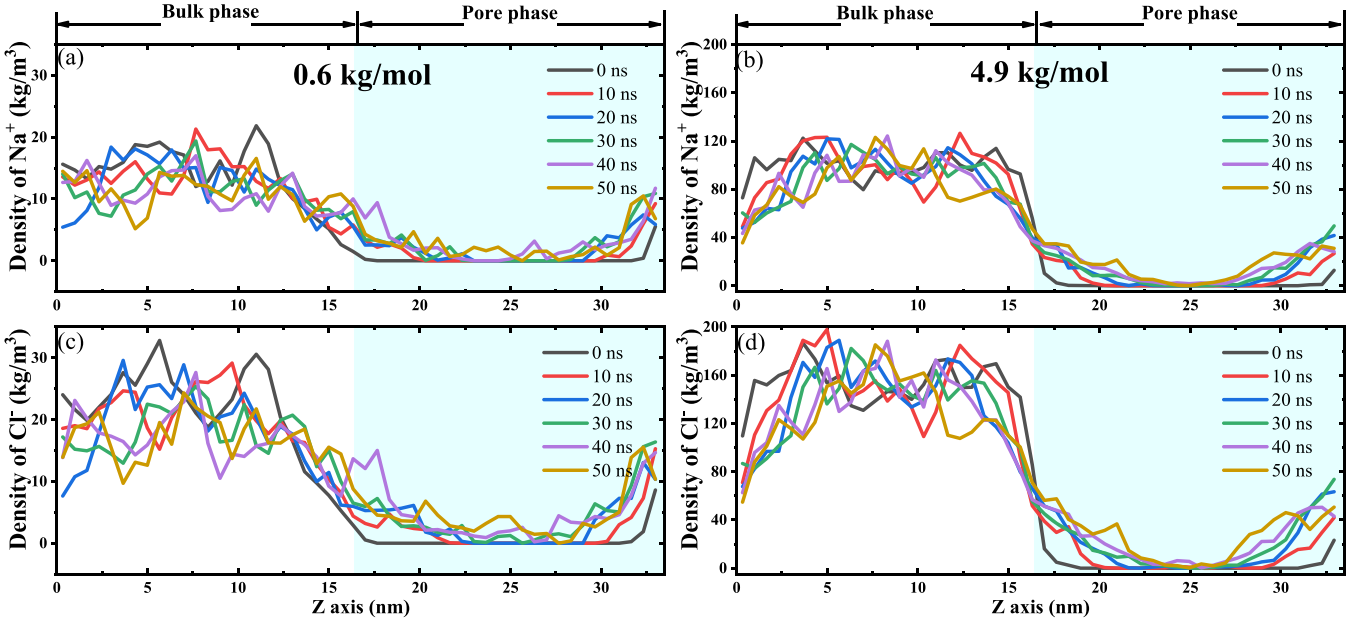

Figure 8. Density profiles of Na^+ (a, b) and Cl^- (c, d) along the pore directions in both simulation systems at different simulation times.

decrease in the diffusion coefficient in the high-concentration solution. Furthermore, we define a time autocorrelation function $R(t)$, which is used to calculate the characteristic residence times τ of Na^+ and Cl^- ions in the inorganic bulk phase, as follows:

$$R(t) = \langle h(t)h(0)\rangle / \langle h(0)^2\rangle \quad (2)$$

where $h(t)$ is the population operator, with a value of 1, indicating that the cations or anions are in the bulk solution phase at time t and a value of 0 indicating ion diffusion into the pore phase. The angular brackets represent an ensemble average of the same cations and anions. The τ values are obtained by fitting the autocorrelation functions of the two systems to a stretched exponential decay, $R(t) = \exp(-(t/\tau)^{\beta})$, where β is the stretching parameter. The τ values of the two ions in the bulk phases are quite large (see Figure 7). Similar to the time-dependent MSD, ions remain in the bulk phase for longer with an increasing ion concentration.

The calculations of the MSDs, RDFs, and time autocorrelation functions of the two ions reveal the same result: increasing the ion concentration does not facilitate ion diffusion from the bulk phase into the pore phase. Instead, the cations and anions generally remain in the bulk phase, and with lower diffusion efficiencies (low proportion) than expected, these ions may interact with the hydrate phase. There may be two reasons for this: (i) the mass effect of the residual hydrate with a high saturability at the initial dissociation stage, and thus, ions cannot diffuse into the space occupied by the solid hydrate. (ii) The water molecules form hydration shells around the ions (Na^+ and Cl^-), which may shield the electric field of the ions and affect their kinetic properties, such as ion transport and conduction. This inhibition effect may be enhanced with increasing ion concentration.[79]

The numbers of ions in the pores increase in the two simulation systems with this diffusion behavior, and substantial time is required to reach the ionic equilibria. Figure 8 shows the ion densities along the Z axes at different simulation times in the two systems. Clearly, at the beginning of ion invasion, few ions are observed in the pore phases, and the numbers of ions in the regions of the pore sides near the bulk phases increase with hydrate dissociation. Most of the pore phases (in the centers of the pore phases) do not contain ions because of the mass effect of the residual hydrate, and thus, only both

https://doi.org/10.1021/acs.energyfuels.2c00978
Energy Fuels 2022, 36, 6216−6228

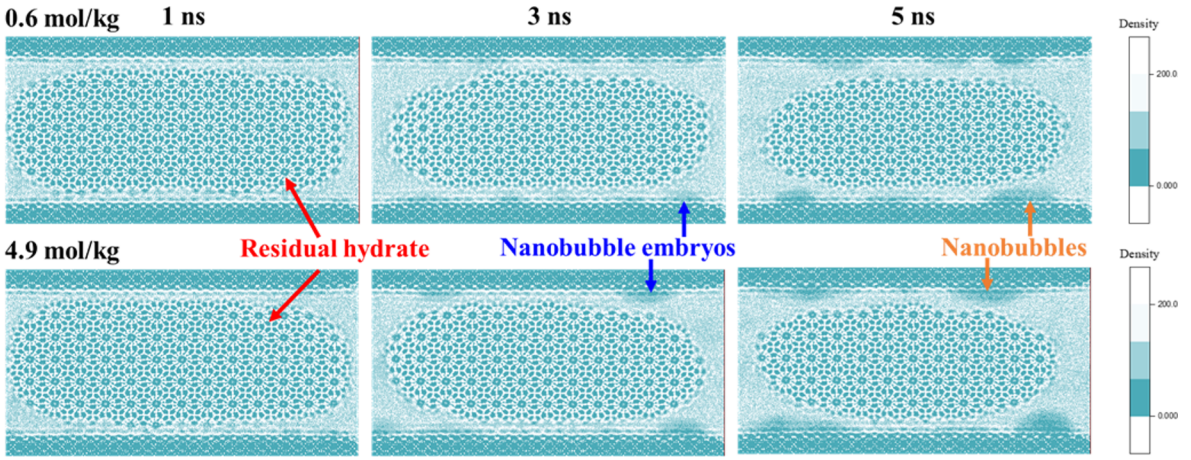

Figure 9. 2D planar number-density maps of the two simulation systems in the *YZ* planes at initial simulation times. Each map is an average of 50 images over 500 ps (1, 3, and 5 ns). Hydrate dissociation in a silica pore in pure water is available,[13] which clearly shows that surface nanobubbles are formed at 5 ns.

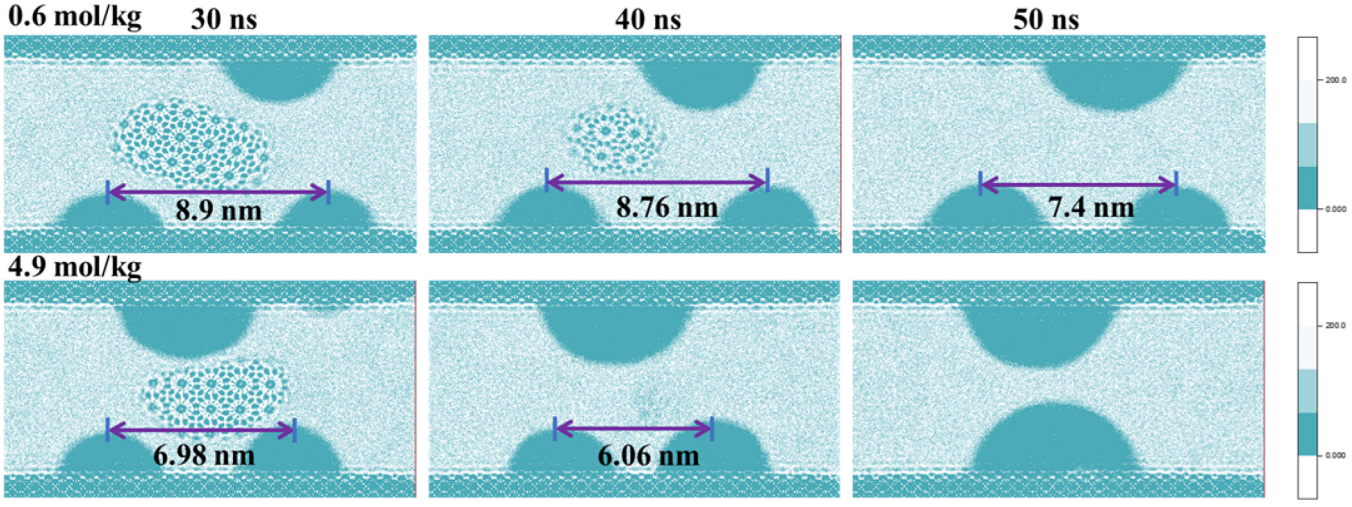

Figure 10. 2D planar number-density maps of the two simulation systems in the *YZ* plane at the middle and late stages of dissociation. Each map consists of an average of 50 images over 500 ps (30, 40, and 50 ns).

sides of the hydrate in the pore direction are exposed to the salt solution and maintain large surfaces facing the solid phases at this stage. When hydrate dissociation occurs, ions gradually permeate into the pore, leading to residual hydrate phase immersion in the salt solution until dissociation is complete. Although more ions diffuse into the pore phase in the system with a high NaCl concentration, the ion invasion processes are similar.

In general, few ions are observed in the pore phase at the initial simulation time, with the numbers of ions in the pores increasing over time in both simulation systems. For comparison, the number of ions permeating from outside the pore may be increased with increasing NaCl concentration, but the diffusion efficiency decreases. Most ions remain in the bulk phase with large τ values until the simulation is completed in both systems because of the ion hydration effects. Conversely, ion invasion is clearly shown in Figure 8. Initially, only the hydrate surfaces face the bulk phase on both sides of the pore exposed to the salt solution, and the residual hydrate undergoes stepwise immersion in the salt solution, with ion diffusion and hydrate dissociation. The salt ions diffuse very slowly in the water layer between hydrate silica throughout the hydrate dissociation process, and this phenomenon is mainly caused by the stereo-hindrance effect of the undissociated hydrate phase (the confinement effect of the pore also influences the diffusion of ions, but the effect is not significant; detailed analyses are shown in the Supporting Information). Therefore, the ion diffusion characteristics should be fully considered during salt addition in gas production from hydrate reservoirs in marine sediments.

3.3. Effects of Ion Invasion on Hydrate Dissociation.

According to the simulation results of Yagasaki et al.,[10] a NaCl solution enhances hydrate dissociation in a liquid phase by accelerating nanobubble formation. A dense NaCl solution induces nanobubble formation close to the hydrate surface. To investigate nanobubble formation, we computed 2D planar number-density maps for the two simulation systems in the *YZ* planes at initial simulation times (1, 3, and 5 ns), as shown in Figure 9. Owing to the large differences in density, the three phases, including solid (residual hydrate and silica), liquid, and gas (methane), may be clearly identified.

Compared to the density maps and our previous simulation results,[13] there are no clear nanobubbles observed at 1 ns. After 2 ns dissociation, several gas clusters (nanobubble embryos)

https://doi.org/10.1021/acs.energyfuels.2c00978
Energy Fuels 2022, 36, 6216−6228

form on the solid surface, and at 5 ns, nanobubbles are clearly observed. The simulation results indicate that NaCl invasion plays a minor role in nanobubble formation during the initial hydrate dissociation because the ions rarely diffuse into the pores and interact only with both sides of the hydrate phase along the pore direction. During this initial period, a large amount of methane escapes from the hydrate surface, which is close to the pore entrances that interface with the bulk phase owing to the PBCs. Compared to the pore size, more methane is released from the large proportion of the hydrate surface facing the silica slabs—there are only thin water layers between the solid and hydrate phases, and methane may cross the water layers easily due to the fugacity difference and aggregate on the solid surface due to steric hindrance. Therefore, the effects of confinement and the surface may be the main causes of nanobubble formation—nanobubbles grow on the solid surface, but the NaCl solution enhancing hydrate dissociation via swift nanobubble formation is not completely reflected. With hydrate dissociation, ions diffuse into the pore, the liquid phase surrounding the residual hydrate changes from pure water to NaCl solution, and the concentration is increased. Hence, the invasion of NaCl solution may decrease the solubility of methane, inhibit methane diffusion from the solid to the liquid phase, and decelerate hydrate dissociation (Figure 4).[11]

The concentration of NaCl in the bulk phase plays a minor role in nanobubble formation as the hydrate dissociates. Although NaCl invasion cannot facilitate hydrate dissociation within the silica pore, it exhibits an effect on the growth and motion of the surface nanobubbles. In both systems, nanobubbles on the solid surface generally approach one another, which is clearer in the system with a high NaCl concentration. This is clearly shown by the 2D planar number-density maps of the simulation systems in the *YZ* plane at the middle and later times in the simulations displayed in Figure 10. This occurs because ion invasion may enhance the hydrophobic interactions between methane molecules and cause a highly non-uniform distribution of dissolved methane molecules,[11] resulting in a decreased methane solubility in the liquid phase. This methane generally diffuses into the gas phase (nanobubbles), and nanobubbles grow toward the origin of methane (residual hydrate phase) and finally manifest a specific directional nanobubble growth toward the center of the pore due to the PBC. More ions diffuse into the pore space during the simulation in the system with a high NaCl concentration, although the diffusion efficiency is less than that in the system with a low NaCl concentration. This specific directional growth effect may be enhanced compared to that of the other system (and was not previously observed in the hydrate dissociation system without NaCl solution[13]). The density distributions in the pore direction are shown in Figure 11, in which the motion of the nanobubbles is clearly indicated. Because of the directional motion of the nanobubbles in the system with a high NaCl concentration, the nanobubbles are closer to the residual hydrate, leading to a more rapid hydrate dissociation than that in the system with a low NaCl concentration. In addition, the two surface nanobubbles merge after hydrate dissociated due to PBC simulation conditions.

3.4. Gas/Water Production. Under static conditions, the released methane may be divided into two fractions: one fraction, the residual gas, remains in the nanopore, and the other may diffuse out of the pore, which is the natural gas

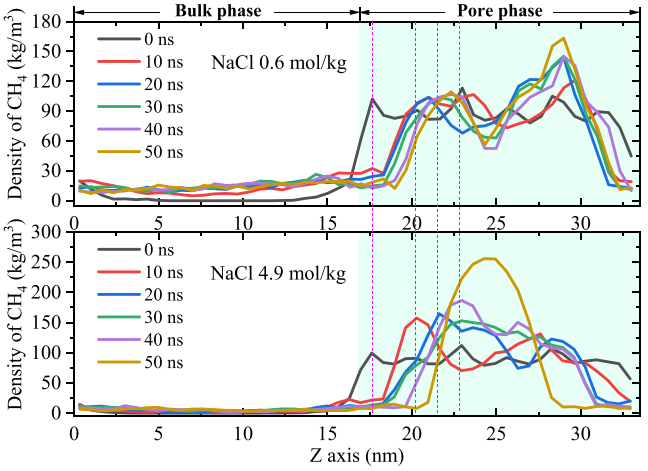

Figure 11. Density distributions of methane in the *Z* direction at different simulation times in the two systems. The density distribution in the pore direction remains similar after 10 ns in the system with a low NaCl concentration. The density distribution changes, with the density in the center of the pore increasing and those at both mouths of the pore decreasing.

extracted from the hydrate reservoirs. To improve the gas production efficiency, the amount of diffused methane should be increased, and the residual methane decreased. Similar to our simulations,[13] the diffusion of methane from the nanopore to the bulk phase is driven by molecular thermal motion and concentration gradients in sediments with low permeabilities. Generally, salts (including NaCl) are added to promote gas production by shifting the phase equilibrium pressure−temperature curve. However, the simulation results reveal that ion invasion from outer pores negatively affects the rate of hydrate dissociation within the nanopore, which is also experimentally observed.[6] To quantify the effect of ion invasion on hydrate dissociation within the nanopore, the variation in the numbers of methane and water molecules outside the pore with time was recorded, as shown in Figure 12.

The amounts of methane in the bulk phases increase rapidly, reaching extrema within the initial several nanoseconds in the three dissociation systems, and maintain dynamic equilibria. This is because the bulk phase initially contains less methane. With dissociation, numerous methane molecules are released from the solid hydrate phase and diffuse out of the pores, driven by the large methane concentration gradient. Because the simulations are performed in an adiabatic ensemble, increasing methane in the bulk phases decreases the methane concentration gradients until equilibrium. Figure 12 shows that the higher NaCl concentration of the aqueous solution external to the pore results in a rapid decrease in the methane leaving the pore. Additionally, the diffusion of methane in the solution with a high salt concentration is restrained due to the low solvent mobility.[80] As for the system with a low NaCl concentration, the diffusion is slightly lower than that in the pure water system because of the low initial dissociation rate. The diffusion is then enhanced with hydrate dissociation and ion diffusion from the bulk to the pore phase. Subsequently, the methane number in the bulk phase decreases due to the low solubility in NaCl solution. Also, the diffusion of released water molecules is hindered by the NaCl solution owing to the hydration effects, with this inhibitory effect enhanced by the NaCl concentration.

https://doi.org/10.1021/acs.energyfuels.2c00978
Energy Fuels 2022, 36, 6216−6228

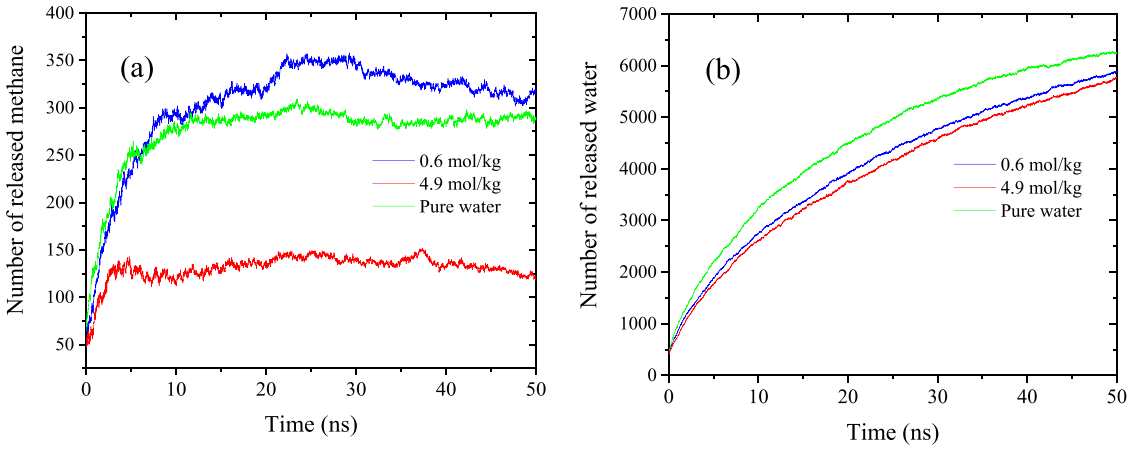

Figure 12. Released methane number (a) and released water number (b) in the bulk phases in the three simulation systems as a function of time (the results of the pure water system are from ref 13). During equilibration prior to molecular dynamics simulation, the hydrate phase dissociates, and thus, several escaped methane and water molecules diffuse into the bulk phase.

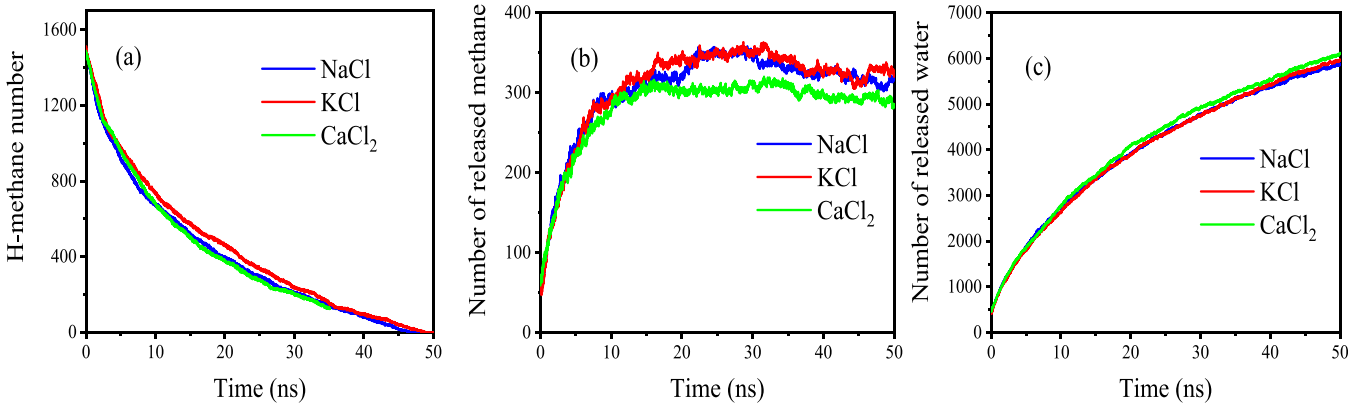

Figure 13. Time evolution of the numbers of methane molecules in the hydrate phases for different salts (a) as well as the numbers of released methane (b) and water (c) molecules in the bulk phases.

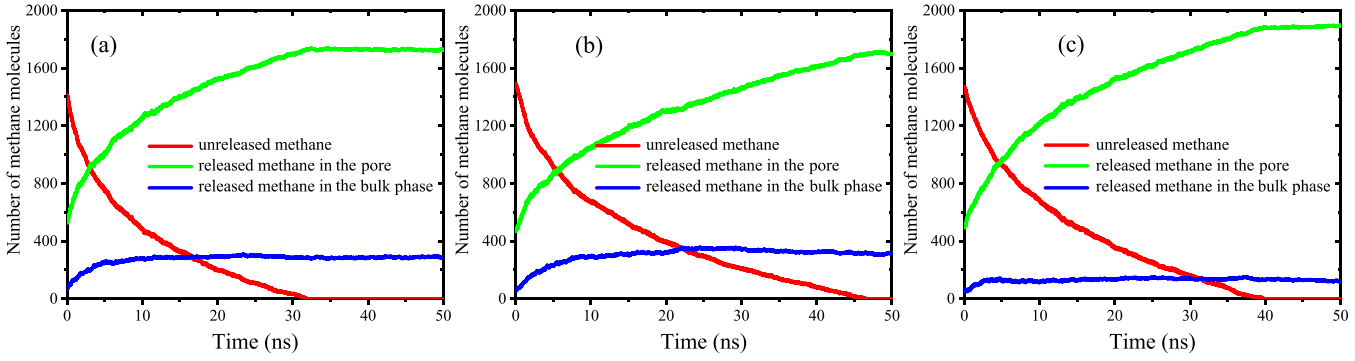

Figure 14. Methane molecules in the simulation systems may be divided into three fractions: remaining in the solid phase (unreleased methane), released and remaining in the pore, and released and diffused out of the pore. Here, the variations with time of the three fractions of methane molecules are shown for the pure water system (a)[13] and 0.6 (b) and 4.9 mol/kg (c) NaCl systems.

3.5. Effects of Cations on Hydrate Dissociation. Compared to Na^+, seawater contains higher contents of K^+ and Ca^{2+}. These ions can be considered as potential additives in hydrate exploitation due to their green features. Therefore, the effects of these cations on hydrate dissociation at the same mass fraction were also analyzed. We constructed two other dissociation systems: the salt (KCl or $CaCl_2$) was added to the bulk phase (3.5 wt %, approximately equal to 0.6 mol/kg for the NaCl solution). Other simulation details were identical to those of the NaCl solutions as described in the Materials and Methods section. The variations of the numbers of methane molecules in the solid phases with time are shown in Figure 13. There is no significant difference in the dissociation rate when different ions are added to the aqueous phase external to the pore at the same low fraction (3.5 wt %) at 292 K. The ion invasion effect may inhibit hydrate dissociation within the pore, independent of the type of cations external to the pore under the simulation conditions, and the gas and water

https://doi.org/10.1021/acs.energyfuels.2c00978
Energy Fuels 2022, 36, 6216−6228

migration are also similar. Therefore, the confinement and surface may be the main factors governing hydrate dissociation and water/gas migration under the simulation conditions.

4. DISCUSSION

In our simulations, salt invasion mainly reveals a negative effect on hydrate dissociation within the silica pore under heating because the salt solution cannot permeate into the pore sufficiently in the initial phase of hydrate dissociation. The confined space and surface hinder the diffusion of the released methane, leading to nanobubble formation. Therefore, salt solutions have no obvious positive effect on nanobubble formation but maintain the negative effect on hydrate dissociation when ions gradually diffuse into the nanopore as the hydrate dissociates under the simulation static environments. To improve the positive effect of the salt solution, a sufficient flow of salt solution to the NGH reservoir is required at the primary stage of hydrate dissociation, enabling the immersion of the hydrate phase in the salt solution throughout hydrate dissociation.

In nature, abundant gas hydrate resources occur in the pores and slits formed by sand and clay mineral particles in marine sediments.[5] Numerous studies report that confinement and solid surfaces within pores may shift the phase equilibrium curves of hydrates[81,82] and affect the dynamic behavior in hydrate formation and dissociation.[20] In addition, the confinement and surface may induce additional capillary pressure within the pore, which considerably affects the water and gas flow and decreases the effective permeability.[83] In our MD simulations, most of the released methane molecules clearly remain within the pores as nanobubbles adsorbed on the solid surfaces (Figures 3 and 14). The surface adsorption in the simulations is relatively stable and reduces the gas production efficiency. The confinement and solid surface properties may weaken the particle exchange capacity for methane molecules and ions under the simulation conditions. The key problems of gas production in hydrate reservoirs using heating with salt addition are the effective improvement of diffusion and effective permeability into solution.

5. CONCLUSIONS

To investigate the effects of ion invasion on hydrate dissociation under sediment conditions where hydrate resources often occur, initial configurations comprising bulk (with a low or high NaCl concentration) phases and hydrate phases within the silica phases were studied using MD simulations in the NVE ensemble at an initial temperature of 292 K. In the simulations, ion invasion from the bulk phase external to the pore could decrease hydrate dissociation within the nanopore. This originated from the invasion characteristics of ions from the bulk to the pore phase. In the initial stage of dissociation, few ions diffused into the pore from the bulk phase. These ions only interacted with a small fraction of the hydrate phase at the two sides of the pore in the systems with low or high NaCl concentrations. At this stage, ion invasion played a minor role in nanobubble formation, and the confined space and surface properties were the main factors governing the hydrate phase change and formation of surface nanobubbles. Subsequently, the number of ions in the pore phase gradually increased until hydrate dissociation was complete, and ions permeated the pore phase around the residual hydrate, thereby decreasing the methane diffusion rate. This implies that the rate of dissociation of the hydrate phase was reduced compared to that observed in the pure water system.[13] Compared to the system with a low NaCl concentration, more ions could migrate into the pore in the system with a high NaCl concentration, leading to surface nanobubble growth in the residual hydrate direction, with the nanobubble closer to the hydrate phase accommodating the dissolved methane and accelerating the dissociation. The salt invasion did not alter the manner of hydrate dissociation, and the hydrate in the nanopore exhibited stepwise dissociation, forming nanobubbles on the solid surface under simulation conditions similar to those of dissociation in the pure water system.[13] Additionally, the solution with a high NaCl concentration outside the pore significantly decreased the migration of released methane molecules toward the bulk phase.

This study revealed the remarkable effect of ion invasion on the dissociation of methane hydrate within sand pores. The simulation results were unexpected as salt addition did not promote hydrate dissociation under the simulation conditions, and the negative effect of salt in gas hydrate extraction should be considered. In summary, hydrate dissociation in sediments could be affected by multiple factors, such as confined space, surface properties, driving force, and ionic additives, all of which could affect hydrate dissociation. Prior to gas production from hydrate reservoirs, these factors should be comprehensively considered to ensure enhanced efficiency and increased gas production.

■ ASSOCIATED CONTENT

Supporting Information

The Supporting Information is available free of charge at https://pubs.acs.org/doi/10.1021/acs.energyfuels.2c00978.

MSDs and diffusion coefficients of the Na^+ cation and Cl^- anion in the two simulation systems (PDF)

■ AUTHOR INFORMATION

Corresponding Authors

Tao Lü − *School of Automation, China University of Geosciences, Wuhan 430074, China; Hubei Key Laboratory of Advanced Control and Intelligent Automation for Complex Systems, Wuhan 430074, China;* orcid.org/0000-0002-6317-8039; Email: lvtaohn@126.com

Fulong Ning − *Faculty of Engineering, China University of Geosciences, Wuhan, Hubei 430074, China; National Center for International Research on Deep Earth Drilling and Resource Development, China University of Geosciences, Wuhan 430074, China; Laboratory for Marine Mineral Resources, Qingdao National Laboratory for Marine Science and Technology, Qingdao 266237, China;* orcid.org/0000-0003-1236-586X; Email: nflzx@cug.edu.cn

Authors

Bin Fang − *School of Mathematics and Physics, China University of Geosciences, Wuhan 430074, China; Process and Energy Department, Delft University of Technology, Delft 2628CB, The Netherlands; National Center for International Research on Deep Earth Drilling and Resource Development, China University of Geosciences, Wuhan 430074, China*

Liwei Cheng − *Faculty of Engineering, China University of Geosciences, Wuhan, Hubei 430074, China; National Center for International Research on Deep Earth Drilling and*

https://doi.org/10.1021/acs.energyfuels.2c00978
Energy Fuels 2022, 36, 6216−6228

Resource Development, China University of Geosciences, Wuhan 430074, China

Dongdong Wang − *Faculty of Engineering, China University of Geosciences, Wuhan, Hubei 430074, China; National Center for International Research on Deep Earth Drilling and Resource Development, China University of Geosciences, Wuhan 430074, China*

Yang Ni − *School of Mathematics and Physics, China University of Geosciences, Wuhan 430074, China*

Bowen Fan − *School of Mathematics and Physics, China University of Geosciences, Wuhan 430074, China*

Jiuling Meng − *School of Mathematics and Physics, China University of Geosciences, Wuhan 430074, China*

Thijs J. H. Vlugt − *Process and Energy Department, Delft University of Technology, Delft 2628CB, The Netherlands;* orcid.org/0000-0003-3059-8712

Complete contact information is available at: https://pubs.acs.org/10.1021/acs.energyfuels.2c00978

Notes

The authors declare no competing financial interest.

■ ACKNOWLEDGMENTS

This work was supported by the National Key Research and Development Project (no. 2018YFE0126400), the Key Program of Marine Economy Development (Six Marine Industries) Special Foundation of the Department of Natural Resources of Guangdong Province (GDNRC [2020]047), the Fundamental Research Funds for National Universities, China University of Geosciences (Wuhan) (grant no. CUGGC09), and the National Natural Science Foundation of China (no. 41976203). T.J.H.V. acknowledges NWO for a VICI grant.

■ REFERENCES

(1) Sloan, E. D.; Koh, C. A. *Clathrate hydrates of natural gases*; CRC press, 2007, DOI: 10.1201/9781420008494.

(2) Collett, T. S.; Johnson, A.; Knapp, C. C.; Boswell, R. *Natural Gas Hydrates: Energy Resource Potential and Associated Geologic Hazards, AAPG Memoir 89*; AAPG, 2009, DOI: 10.1306/M891320

(3) Nandanwar, M. S.; Anderson, B. J.; Ajayi, T.; Collett, T. S.; Zyrianova, M. V. Evaluation of gas production potential from gas hydrate deposits in National Petroleum Reserve Alaska using numerical simulations. *J. Nat. Gas Sci. Eng.* **2016**, *36*, 760−772.

(4) Li, X. S.; Xu, C. G.; Zhang, Y.; Ruan, X. K.; Li, G.; Wang, Y. Investigation into gas production from natural gas hydrate: A review. *J. Appl. Energy* **2016**, *172*, 286−322.

(5) Boswell, R. Is Gas Hydrate Energy Within Reach? *Science* **2009**, *325*, 957−958.

(6) Nair, V. C.; Ramesh, S.; Ramadass, G. A.; Sangwai, J. S. Influence of thermal stimulation on the methane hydrate dissociation in porous media under confined reservoir. *J. Pet. Sci. Eng.* **2016**, *147*, 547−559.

(7) Wang, J.; Han, F.; Li, S.; Ge, K.; Zheng, Z. Investigation of gas hydrate production with salinity via depressurization and thermal stimulation methods. *J. Pet. Sci. Eng.* **2020**, *194*, 107465.

(8) Maekawa, T.; Itoh, S.; Sakata, S.; Igari, S.; Imai, N. Pressure and Temperature Conditions for Methane Hydrate Dissociation in Sodium-Chloride Solutions. *Geochem. J.* **1995**, *29*, 325−329.

(9) Jager, M. D.; Sloan, E. D. The effect of pressure on methane hydration in pure water and sodium chloride solutions. *Fluid Phase Equilib.* **2001**, *185*, 89−99.

(10) Yagasaki, T.; Matsumoto, M.; Andoh, Y.; Okazaki, S.; Tanaka, H. Dissociation of methane hydrate in aqueous NaCl solutions. *J. Phys. Chem. B* **2014**, *118*, 11797−11804.

(11) Yagasaki, T.; Matsumoto, M.; Tanaka, H. Effects of thermodynamic inhibitors on the dissociation of methane hydrate: a molecular dynamics study. *Phys. Chem. Chem. Phys.* **2015**, *17*, 32347−32357.

(12) Xu, J.; Gu, T.; Sun, Z.; Li, X.; Wang, X. Molecular dynamics study on the dissociation of methane hydrate via inorganic salts. *Mol. Phys.* **2016**, *114*, 34−43.

(13) Fang, B.; Ning, F.; Ou, W.; Wang, D.; Zhang, Z.; Yu, Y.; Lu, H.; Wu, J.; Vlugt, T. J. H. The dynamic behavior of gas hydrate dissociation by heating in tight sandy reservoirs: A molecular dynamics simulation study. *Fuel* **2019**, *258*, 116106.

(14) Nguyen, N. N.; Galib, M.; Nguyen, A. V. Critical Review on Gas Hydrate Formation at Solid Surfaces and in Confined Spaces - Why and How Does Interfacial Regime Matter? *Energy Fuels* **2020**, *34*, 6751−6760.

(15) Theodorakis, P. E.; Che, Z. Surface nanobubbles: Theory, simulation, and experiment. A review. *Adv. Colloid Interface Sci.* **2019**, *272*, 101995.

(16) Zhou, J.; Liang, W.; Wei, C. Phase Equilibrium Condition for Pore Hydrate: Theoretical Formulation and Experimental Validation. *J. Geophys. Res.: Solid Earth* **2019**, *124*, 12703−12721.

(17) Jensen, L.; Thomsen, K.; von Solms, N.; Wierzchowski, S.; Walsh, M. R.; Koh, C. A.; Sloan, E. D.; Wu, D. T.; Sum, A. K. Calculation of liquid water-hydrate-methane vapor phase equilibria from molecular simulations. *J. Phys. Chem. B* **2010**, *114*, 5775−5782.

(18) Conde, M. M.; Vega, C. Determining the three-phase coexistence line in methane hydrates using computer simulations. *J. Chem. Phys.* **2010**, *133*, No. 064507.

(19) Conde, M. M.; Vega, C.; McBride, C.; Noya, E. G.; Ramírez, R.; Sesé, L. M. Can gas hydrate structures be described using classical simulations? *J. Chem. Phys.* **2010**, *132*, 114503.

(20) Jin, D.; Coasne, B. Reduced phase stability and faster formation/dissociation kinetics in confined methane hydrate. *Proc. Natl. Acad. Sci. U. S. A.* **2021**, *118*, No. e2024025118.

(21) Khurana, M.; Yin, Z.; Linga, P. A Review of Clathrate Hydrate Nucleation. *ACS Sustainable Chem. Eng.* **2017**, *5*, 11176−11203.

(22) Walsh, M. R.; Beckham, G. T.; Koh, C. A.; Sloan, E. D.; Wu, D. T.; Sum, A. K. Methane Hydrate Nucleation Rates from Molecular Dynamics Simulations: Effects of Aqueous Methane Concentration, Interfacial Curvature, and System Size. *J. Phys. Chem. C* **2011**, *115*, 21241−21248.

(23) Jacobson, L. C.; Molinero, V. Can amorphous nuclei grow crystalline clathrates? The size and crystallinity of critical clathrate nuclei. *J. Am. Chem. Soc.* **2011**, *133*, 6458−6463.

(24) Debenedetti, P. G.; Sarupria, S. Hydrate molecular ballet. *Science* **2009**, *326*, 1070−1071.

(25) Moon, C.; Taylor, P. C.; Rodger, P. M. Molecular dynamics study of gas hydrate formation. *J. Am. Chem. Soc.* **2003**, *125*, 4706−4707.

(26) Radhakrishnan, R.; Trout, B. L. A new approach for studying nucleation phenomena using molecular simulations: Application to CO2 hydrate clathrates. *J. Chem. Phys.* **2002**, *117*, 1786−1796.

(27) Knott, B. C.; Molinero, V.; Doherty, M. F.; Peters, B. Homogeneous nucleation of methane hydrates: unrealistic under realistic conditions. *J. Am. Chem. Soc.* **2012**, *134*, 19544−19547.

(28) Vatamanu, J.; Kusalik, P. G. Unusual crystalline and polycrystalline structures in methane hydrates. *J. Am. Chem. Soc.* **2006**, *128*, 15588−15589.

(29) Liang, S.; Kusalik, P. G. Crystal growth simulations of H_2S hydrate. *J. Phys. Chem. B* **2010**, *114*, 9563−9571.

(30) Oluwunmi, P. A.; Finney, A. R.; Rodger, P. M. Molecular dynamics screening for new kinetic inhibitors of methane hydrate. *Can. J. Chem.* **2015**, *93*, 1043−1049.

(31) Bagherzadeh, S. A.; Alavi, S.; Ripmeester, J. A.; Englezos, P. Why ice-binding type I antifreeze protein acts as a gas hydrate crystal inhibitor. *Phys. Chem. Chem. Phys.* **2015**, *17*, 9984−9990.

(32) Yagasaki, T.; Matsumoto, M.; Tanaka, H. Adsorption of Kinetic Hydrate Inhibitors on Growing Surfaces: A Molecular Dynamics Study. *J. Phys. Chem. B* **2018**, *122*, 3396−3406.

(33) Phan, A.; Bui, T.; Acosta, E.; Krishnamurthy, P.; Striolo, A. Molecular mechanisms responsible for hydrate anti-agglomerant performance. *Phys. Chem. Chem. Phys.* **2016**, *18*, 24859−24871.
(34) Bui, T.; Phan, A.; Monteiro, D.; Lan, Q.; Ceglio, M.; Acosta, E.; Krishnamurthy, P.; Striolo, A. Evidence of Structure-Performance Relation for Surfactants Used as Antiagglomerants for Hydrate Management. *Langmuir* **2017**, *33*, 2263−2274.
(35) Bellucci, M. A.; Walsh, M. R.; Trout, B. L. Molecular Dynamics Analysis of Anti-Agglomerant Surface Adsorption in Natural Gas Hydrates. *J. Phys. Chem. C* **2018**, *122*, 2673−2683.
(36) Bertolazzo, A. A.; Naullage, P. M.; Peters, B.; Molinero, V. The Clathrate-Water Interface Is Oleophilic. *J. Phys. Chem. Lett.* **2018**, *9*, 3224−3231.
(37) Jiménez-Ángeles, F.; Firoozabadi, A. Hydrophobic Hydration and the Effect of NaCl Salt in the Adsorption of Hydrocarbons and Surfactants on Clathrate Hydrates. *ACS Cent. Sci.* **2018**, *4*, 820−831.
(38) English, N. J.; Tse, J. S. Mechanisms for thermal conduction in methane hydrate. *Phys. Rev. Lett.* **2009**, *103*, No. 015901.
(39) Peters, B.; Zimmermann, N. E. R.; Beckham, G. T.; Tester, J. W.; Trout, B. L. Path sampling calculation of methane diffusivity in natural gas hydrates from a water-vacancy assisted mechanism. *J. Am. Chem. Soc.* **2008**, *130*, 17342−17350.
(40) Wu, Z.; Liu, W.; Zheng, J.; Li, Y. Effect of methane hydrate dissociation and reformation on the permeability of clayey sediments. *Appl. Energy* **2020**, *261*, 114479.
(41) Cheng, C.; Zhao, J.; Yang, M.; Liu, W.; Wang, B.; Song, Y. Evaluation of Gas Production from Methane Hydrate Sediments with Heat Transfer from Over-Underburden Layers. *Energy Fuels* **2015**, *29*, 1028−1039.
(42) Jung, J. W.; Jang, J.; Santamarina, J. C.; Tsouris, C.; Phelps, T. J.; Rawn, C. J. Gas Production from Hydrate-Bearing Sediments: The Role of Fine Particles. *Energy Fuels* **2012**, *26*, 480−487.
(43) Li, X. Y.; Li, X. S.; Wang, Y.; Zhang, Y.; Wan, K.; Zeng, H. P. The consistency of the normalized hydrate dissociation rate in the hydrate simulator with different scales. *Fuel* **2021**, *287*, 119436.
(44) Zhang, Z.; Li, C.; Ning, F.; Liu, L.; Cai, J.; Liu, C.; Wu, N.; Wang, D. Pore Fractal Characteristics of Hydrate-Bearing Sands and Implications to the Saturated Water Permeability. *J. Geophys. Res.: Solid Earth* **2020**, *125*, No. e2019JB018721.
(45) Yin, Z.; Moridis, G.; Chong, Z. R.; Tan, H. K.; Linga, P. Numerical analysis of experiments on thermally induced dissociation of methane hydrates in porous media. *Ind. Eng. Chem. Res.* **2017**, *57*, 5776.
(46) Kwon, T.-H.; Cho, G.-C.; Santamarina, J. C. Gas hydrate dissociation in sediments: Pressure-temperature evolution. *Geochem., Geophys., Geosyst.* **2008**, *9*, Q03019.
(47) Fang, B.; Lü, T.; Ning, F.; Pang, J.; He, Z.; Sun, J. Facilitating gas hydrate dissociation kinetics and gas migration in clay interlayer by surface cations shielding effects. *Fuel* **2022**, *318*, 123576.
(48) Chaouachi, M.; Falenty, A.; Sell, K.; Enzmann, F.; Kersten, M.; Haberthür, D.; Kuhs, W. F. Microstructural evolution of gas hydrates in sedimentary matrices observed with synchrotron X-ray computed tomographic microscopy. *Geochem., Geophys., Geosyst.* **2015**, *16*, 1711−1722.
(49) He, Z.; Linga, P.; Jiang, J. CH_4 Hydrate Formation between Silica and Graphite Surfaces: Insights from Microsecond Molecular Dynamics Simulations. *Langmuir* **2017**, *33*, 11956−11967.
(50) Bai, D.; Chen, G.; Zhang, X.; Sum, A. K.; Wang, W. How Properties of Solid Surfaces Modulate the Nucleation of Gas Hydrate. *Sci. Rep.* **2015**, *5*, 1−12.
(51) Liang, S.; Kusalik, P. G. The nucleation of gas hydrates near silica surfaces. *Can. J. Chem.* **2015**, *93*, 791−798.
(52) Takeuchi, F.; Hiratsuka, M.; Ohmura, R.; Alavi, S.; Sum, A. K.; Yasuoka, K. Water proton configurations in structures I, II, and H clathrate hydrate unit cells. *J. Chem. Phys.* **2013**, *138*, 124504.
(53) Downs, R. T.; Hall-Wallace, M. The American mineralogist crystal structure database. *Am. Mineral.* **2003**, *88*, 247−250.
(54) Hess, B.; Kutzner, C.; van der Spoel, D.; Lindahl, E. GROMACS 4: Algorithms for highly efficient, load-balanced, and scalable molecular simulation. *J. Chem. Theory Comput.* **2008**, *4*, 435−447.
(55) Abraham, M. J.; Murtola, T.; Schulz, R.; Páll, S.; Smith, J. C.; Hess, B.; Lindahl, E. GROMACS: High performance molecular simulations through multi-level parallelism from laptops to supercomputers. 2015, *1-2* (C), 19−25, DOI: 10.1016/j.softx.2015.06.001.
(56) Berendsen, H. J. C.; Grigera, J. R.; Straatsma, T. P. The missing term in effective pair potentials. *J. Phys. Chem.* **1987**, *91*, 6269−6271.
(57) Martin, M. G.; Siepmann, J. I. Transferable potentials for phase equilibria. 1. United-atom description of n-alkanes. *J. Phys. Chem. B* **1998**, *102*, 2569−2577.
(58) Chandrasekhar, J.; Spellmeyer, D. C.; Jorgensen, W. L. Energy component analysis for dilute aqueous solutions of lithium(1+), sodium(1+), fluoride(1-), and chloride(1-) ions. *J. Am. Chem. Soc.* **1984**, *106*, 903−910.
(59) Lopes, P. E. M.; Murashov, V.; Tazi, M.; Demchuk, E.; MacKerell, A. D. Development of an empirical force field for silica. Application to the quartz-water interface. *J. Phys. Chem. B* **2006**, *110*, 2782−2792.
(60) Ratner, M. A. Understanding molecular simulation: From algorithms to applications, by Daan Frenkel and Berend Smit. *Phys. Today* **1997**, *50*, 66.
(61) Essmann, U.; Perera, L.; Berkowitz, M. L.; Darden, T.; Lee, H.; Pedersen, L. G. A Smooth Particle Mesh Ewald Method. *J. Chem. Phys.* **1995**, *103*, 8577−8593.
(62) Zimmermann, K. Oral - All Purpose Molecular Mechanics Simulator and Energy Minimizer. *J. Comput. Chem.* **1991**, *12*, 310−319.
(63) Bussi, G.; Donadio, D.; Parrinello, M. Canonical sampling through velocity rescaling. *J. Chem. Phys.* **2007**, *126*, No. 014101.
(64) Parrinello, M.; Rahman, A. Polymorphic transitions in single crystals: A new molecular dynamics method. *J. Appl. Phys.* **1981**, *52*, 7182−7190.
(65) Baez, L. A.; Clancy, P. Computer-Simulation of the Crystal-Growth and Dissolution of Natural-Gas Hydrates. *Int. Conf. Nat. Gas Hydrates* **1994**, *715*, 177−186.
(66) Uttormark, M. J.; Thompson, M. O.; Báez, L. A.; Clancy, P. Solid/Liquid Cluster Recognition in Heterogeneous Systems. *Mol. Simul.* **1993**, *11*, 121−144.
(67) Yagasaki, T.; Matsumoto, M.; Andoh, Y.; Okazaki, S.; Tanaka, H. Effect of bubble formation on the dissociation of methane hydrate in water: a molecular dynamics study. *J. Phys. Chem. B* **2014**, *118*, 1900−1906.
(68) Bai, D.; Zhang, D.; Zhang, X.; Chen, G. Origin of Self-preservation Effect for Hydrate Decomposition: Coupling of Mass and Heat Transfer Resistances. *Sci. Rep.* **2015**, *5*, 1−13.
(69) Ma, R.; Cao, D.; Zhu, C.; Tian, Y.; Peng, J.; Guo, J.; Chen, J.; Li, X.-Z.; Francisco, J. S.; Zeng, X. C.; et al. Atomic imaging of the edge structure and growth of a two-dimensional hexagonal ice. *Nature* **2020**, *577*, 60−63.
(70) Ding, L. Y.; Geng, C. Y.; Zhao, Y. H.; Wen, H. Molecular dynamics simulation on the dissociation process of methane hydrates. *Mol. Simul.* **2007**, *33*, 1005−1016.
(71) Bagherzadeh, S. A.; Englezos, P.; Alavi, S.; Ripmeester, J. A. Molecular Modeling of the Dissociation of Methane Hydrate in Contact with a Silica Surface. *J. Phys. Chem. B* **2012**, *116*, 3188−3197.
(72) Johnson, C. A. Generalization of the Gibbs-Thomson equation. *Surf. Sci.* **1965**, *3*, 429−444.
(73) Liang, S.; Yi, L.; Liang, D. Molecular Insights into the Homogeneous Melting of Methane Hydrates. *J. Phys. Chem. C* **2014**, *118*, 28542−28547.
(74) Myshakin, E. M.; Jiang, H.; Warzinski, R. P.; Jordan, K. D. Molecular Dynamics Simulations of Methane Hydrate Decomposition. *J. Phys. Chem. A* **2009**, *113*, 1913−1921.
(75) Windmeier, C.; Oellrich, L. R. Theoretical Study of Gas Hydrate Decomposition Kinetics-Model Development. *J. Phys. Chem. A* **2013**, *117*, 10151−10161.
(76) Du, J.; Wang, X.; Liu, H.; Guo, P.; Wang, Z.; Fan, S. Experiments and prediction of phase equilibrium conditions for

https://doi.org/10.1021/acs.energyfuels.2c00978
Energy Fuels 2022, 36, 6216−6228

methane hydrate formation in the NaCl, $CaCl_2$, $MgCl_2$ electrolyte solutions. *Fluid Phase Equilib.* **2019**, *479*, 1−8.
(77) Semenov, A. P.; Stoporev, A. S.; Mendgaziev, R. I.; Gushchin, P. A.; Khlebnikov, V. N.; Yakushev, V. S.; Istomin, V. A.; Sergeeva, D. V.; Vinokurov, V. A. Synergistic effect of salts and methanol in thermodynamic inhibition of sII gas hydrates. *J. Chem. Thermodyn.* **2019**, *137*, 119−130.
(78) Celebi, A. T.; Jamali, S. H.; Bardow, A.; Vlugt, T. J. H.; Moultos, O. A. Finite-size effects of diffusion coefficients computed from molecular dynamics: a review of what we have learned so far. *Mol. Simul.* **2021**, *47*, 831−845.
(79) Peng, J. B.; Cao, D. Y.; He, Z. L.; Guo, J.; Hapala, P.; Ma, R. Z.; Cheng, B. W.; Chen, J.; Xie, W. J.; Li, X. Z.; Jelínek, P.; Xu, L. M.; Gao, Y. Q.; Wang, E. G.; Jiang, Y. The effect of hydration number on the interfacial transport of sodium ions. *Nature* **2018**, *557*, 701−705.
(80) Bai, D.; Wu, Z.; Lin, C.; Zhou, D. The effect of aqueous NaCl solution on methane hydrate nucleation and growth. *Fluid Phase Equilib.* **2019**, *487*, 76−82.
(81) Borchardt, L.; Casco, M. E.; Silvestre-Albero, J. Methane Hydrate in Confined Spaces: An Alternative Storage System. *ChemPhysChem* **2018**, *19*, 1298−1314.
(82) Casco, M. E.; Zhang, E.; Graetz, S.; Krause, S.; Borchardt. Experimental evidence of confined methane hydrate in hydrophilic and hydrophobic model carbons. *J. Phys. Chem. C* **2019**, *123*, 24071−24079.
(83) Liu, X.; Flemings, P. B. Capillary effects on hydrate stability in marine sediments. *J. Geophys. Res.: Solid Earth* **2011**, *116*, No. 07102.

https://doi.org/10.1021/acs.energyfuels.2c00978
Energy Fuels 2022, 36, 6216−6228